Available online at www.sciencedirect.com

SciVerse ScienceDirect

Procedia Engineering 58 (2013) 355 – 362

Procedia Engineering

www.elsevier.com/locate/procedia

The 12th Hypervelocity Impact Symposium

Behind-Armor Fragments from Tungsten Rods Penetrating Steel

S. Bless[1], J. Tolman[1], and J. McDonald[1,2]

[1]Institute for Advanced Technology, The University of Texas at Austin, 3925 W Braker LN STE 400, Austin, TX 78759, US, [2]now at U.S.Army Research Laboratory, Aberdeen PG, MD 21005

Abstract

Damage done by penetrating projectiles is mainly determined by the debris projected behind the target. Debris formation is a stochastic process, and characterization of debris requires a statistical approach. We have developed an analysis tool capable of estimating behind-target debris statistics, including a new experimental technique using x-ray tomography. This technique allows one to obtain statistical data for direction, mass, and shape factor for the thousands of particles generated in a typical impact. Data are reported for 15 mm diameter tungsten alloy rods penetrating steel at nominally 1.7 and 2.0 km/s. Among the observations are that the mass distribution is uncorrelated with angular distribution, and the number of fragments increases while the size of fragments decreases with velocity. The hydrocode EPIC with its mesh-to-particle algorithm was used to calculate debris fields, with the parameters that control fragment size being calibrated from the statistical data on recovered fragments. Good agreement was obtained, provided the normal fragmentation algorithm was suppressed. This allows predictions of relative damage as velocity is changed.

Selection and peer-review under responsibility of the Hypervelocity Impact Society

Keywords: Beind-Armor Debris, fragmentation, EPIC, tomography

1. Introduction

Damage done by penetrating projectiles is mainly determined by the debris projected behind the target, referred to as "behind-armor debris" (BAD). BAD formation is a stochastic process, and characterization of debris requires a statistical approach. The goal of this effort was to develop new experimental and analytical tools capable of estimating behind-target debris statistics and estimating relative damage.

The geometric form of particle fields behind the target is usually treated in the framework proposed by Mayseless [1] and Saucier [2, 3]. Both the target and projectile fragments are presumed to have similar velocities and to lie on the surface of an expanding and propagating truncated ellipsoid. In the framework of [2] the distributions of particle mass and shape are Gaussian. The number of particles as a function of departure angle is described by a Weibull distribution. The distribution of velocity with angle is described by a cosine function. These distributions were assumed to be independent of one another.

There are very few measurements of the statistical properties of BAD that might serve to substantiate the statistical models. Most attempts have been based on a very laborious process of weighing recovered particles (e.g., [4]), and information regarding velocity and direction is lost. Otherwise, data are obtained for perforations in a standard witness plate array, and debris statistics are derived by matching the stochastic descriptions of holes and departure angles.

Likewise, direct modeling of BAD has proven to be quite difficult because of the absence of physically based fragmentation models and the numerical requirement to track thousands of fragments. Two noteworthy attempts using a physical fragmentation model and numerical mesh-to-particle methods, respectively, are described in [5] and [6].

2. Experimental Techniques

Projectiles were made from 91% W-Ni-Co 15 mm in diameter with a length-to-diameter ratio of ten (L/D = 10). They were stabilized with an aluminum boom and flare. The targets were rolled homogeneous armor (RHA) blocks that were 203

1* Corresponding author. Tel. 512-740-4459. Fax 512 471-9096.
E-mail address: sbless@iat.utexas.edu.

Selection and peer-review under responsibility of the Hypervelocity Impact Society
doi:10.1016/j.proeng.2013.05.040

mm on a side and 122 mm thick. Projectiles were launched from a two-stage light-gas gun with a 38 mm launch tube using discarding aluminum sabots. Nominal impact velocities were 1.7 and 2.0 km/s.

Particle analysis was based on x-ray tomography of BAD that was caught in a witness material. Initially the capture medium was medium-density fiberboard (MDF). However, better results were obtained with Sil-950 rubber. Its main advantage is its amenability to being cast. After some trial and error, it was decided to cast the rubber into a mold shaped like a Bundt cake, illustrated in Figure 1. A hole in the center passed particles with departure angles smaller than 5 degrees. This was used because all experiments produce a large number of large and small BAD fragments at small departure angles, and relative damage depends on particles at larger angles. The hole was lined with a steel pipe to prevent scabbing of rubber into this region. Some surface material was dislodged from the rubber, but it could be glued back in place before tomography. The rubber could be easily removed for tomography by pressing on the rear steel plate.

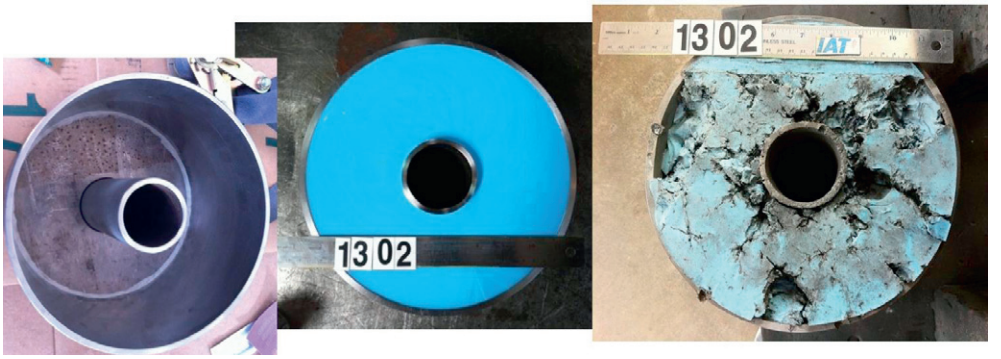

Fig. 1. Placement of capture medium in the steel frame.

The scanning was performed in the high-resolution x-ray computed tomography (XCT) facility at the Department of Geological Sciences at the University of Texas at Austin (UT)—a national, shared multi-user facility supported by the National Science Foundation (NSF) Earth Sciences Directorate (see www.ctlab.geo.utexas.edu). Analysis of XCT data was accomplished with a program written at UT called BLOB. This program was designed to measure three-dimensional geometric information up to thousands of discrete objects, such as behind-armor debris, within a CT data volume. The resolution obtained with these procedures for particle detection was 1 voxel = 0.021 mm^3. Based on the capabilities of the XCT scanning system employed for this study, the analysis could resolve particles down to about 2 mg.

The advantages of XCT are much more than simply saving the time required to recover fragment mass and direction. The technique can also quickly compile data for shape factor, fragment material (steel or tungsten), and presented area, which are the parameters used in damage models [2, 3].

As part of the data reduction process, fragments that were recovered from rubber after a shot were then reshot into the rubber recovery medium in order to obtain a calibration of penetration/(density x diameter) (p/⟩d) vs. velocity (v). The diameter d was taken as the cube root of the volume. The data were fit to a Poncelet equation of the form

$$p/\rho d = A \ln\left[(v/B)^2 + 1\right] \tag{1}$$

Figure 2 shows the results for tungsten and steel fragments, for which the best fit was with the values A = 3.2 cm^3/g and B = 700 m/s.

3. Results

A number of fragments were recovered from the capture medium and polished to examine microstructure. It was found that there were two distinct types of microstructure. In type 1, illustrated in Figure 3A, the interior of grains was relatively undeformed, but the edges exhibited shear zones. In type 2 (Figure 3B) the grains were shredded: all grains were highly deformed and there were interior pores. Type 1 grains are more common and sometimes had boundaries from the original surface of the rod. Therefore, we assume that type 1 grains originate from the outer zones of the penetrator, where material is shed as the rod inverts within the penetration channel.

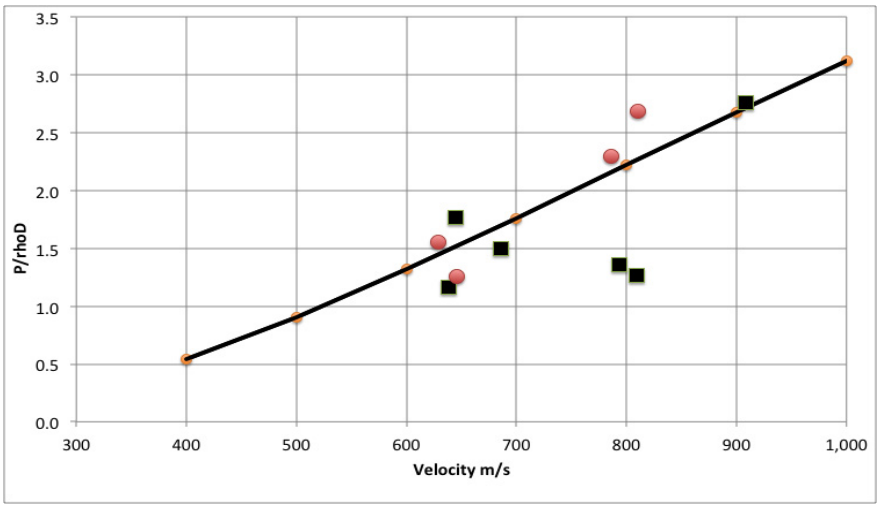

Fig. 2. Velocity calibration of the capture medium. Square points tungsten, round points steel.

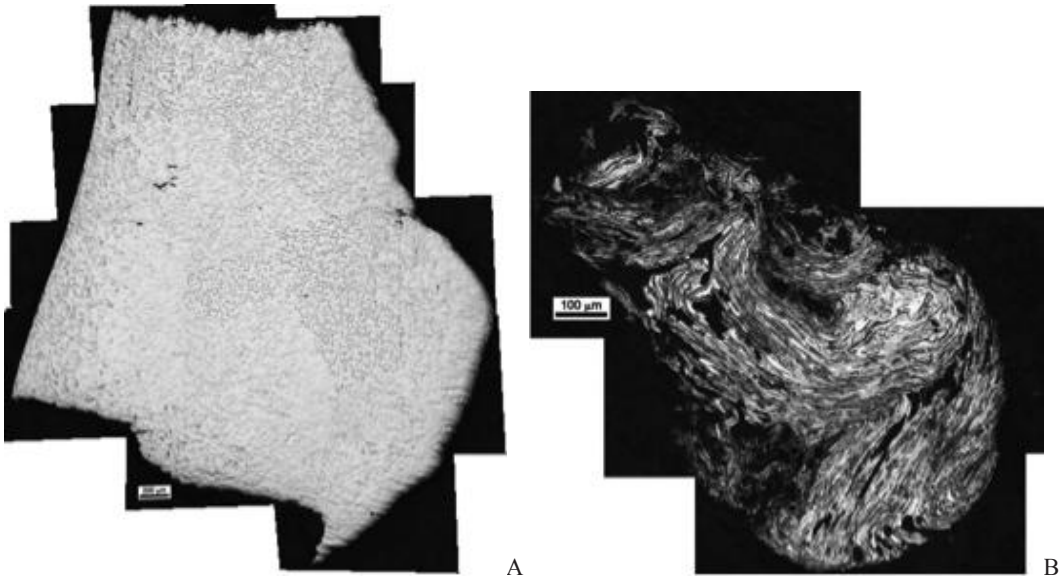

Fig. 3. Examples of the microstructure of recovered grains.

The angular distribution of fragments is shown in Figure 4 for both velocities: Figure 4A is cumulative mass and Figure 4B is cumulative number. There were essentially no fragments beyond a departure angle of 20 degrees. The cone angle is similar in both shots, as can by seen by examining the angle that contains half the mass. In both shots, there is a sharp drop off for angles larger than about 15 degrees. The data in Figure 4 can be fit by a Weibull distribution function, which validates the approach taken by Saucier [2, 3]. There the model for number vs. departure angle \ is

$$N = N_0 \left\{ -\exp\left[-(\theta / b)^c \right] \right\} \quad (2)$$

with c = ln(ln20/ln2)/ln($\lambda_{95}/\lambda_{50}$) and b = $\lambda_{95}/(\ln 20)^{1/c}$, where subscripts 95 and 50 refer to the 95% and 50% cone angles. This model fits the data well, as shown by the dashed line in Figure 4B.

The efficiency of BAD formation can be taken as the ratio of debris mass to mass of rod that was eroded during passage through the target. The eroded mass was measured from after-exit x-rays of the penetrator. The efficiency was 55% at 2.0 km/s and 42% at 1.7 km/s; thus, fragment formation efficiency increases with velocity.

Shapes of particles can be expressed as the shape factor, defined as A(ρ/M)2/3, where A is presented area, M is mass, and ρ is density. The shape factor thus depends on perspective. Shapes are measured by the BLOB program, and from those data a more general description of particle shape can be taken as the aspect ratio R. Particles are fitted to an ellipsoid, and R is the ratio of the largest to the smallest axis. Figure 5 compares aspect ratios of steel and tungsten particles. The steel particles are considerably more elongated than the tungsten particles.

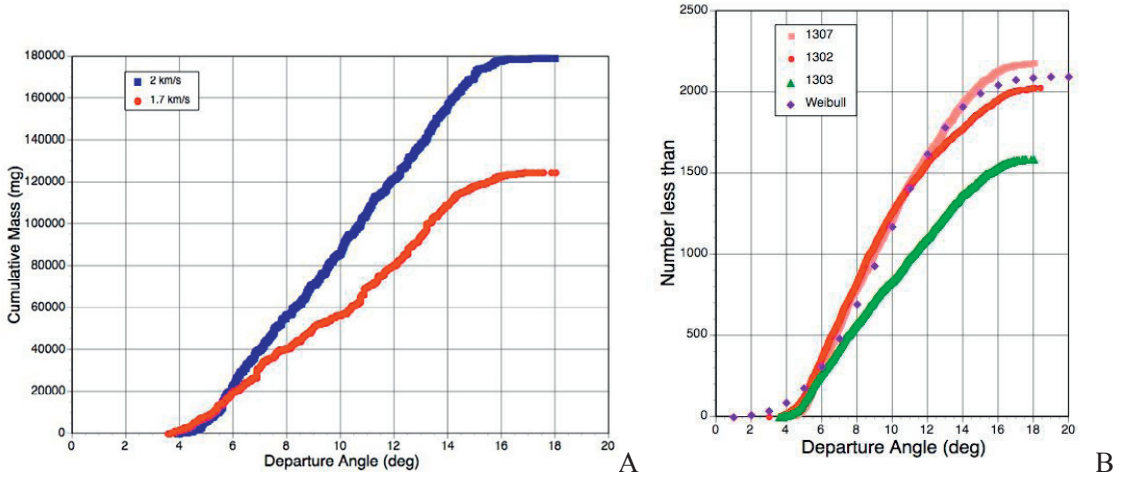

Figure 4. A: cumulative mass as a function of departure angle. B: cumulative number (upper curves are higher velocity).

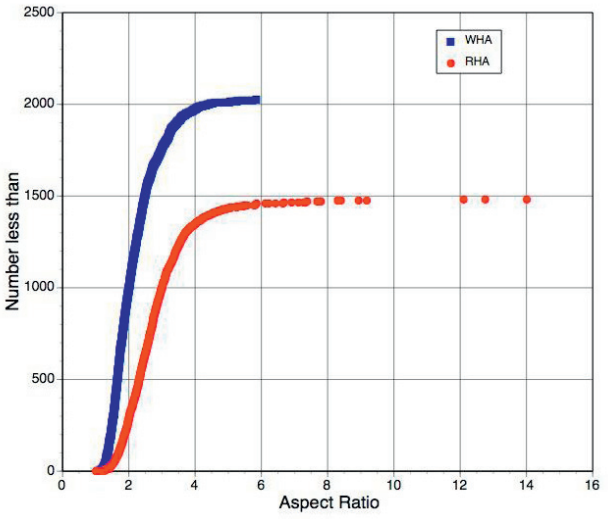

Figure 5. Aspect ratios for tungsten (WHA) and steel (RHA) fragments at 1.7 km/s.

The tungsten fragments are considerably more compact than the steel fragments—both in the average and in the extremes. The Gaussian-type distribution assumed in [2] will tend to underpopulate the low-aspect-ratio fragments for this case.

The mass distribution of tungsten fragments for two shots at 2 km/s and two shots at 1 km/s is shown in Figure 6. The data are reasonably reproducible. The transition from small to large fragments is also reasonably approximated by a Gaussian S-curve, as in [2]. There are many more fragments in the high-velocity shot. However, the low-velocity shot produced a small number of larger fragments.

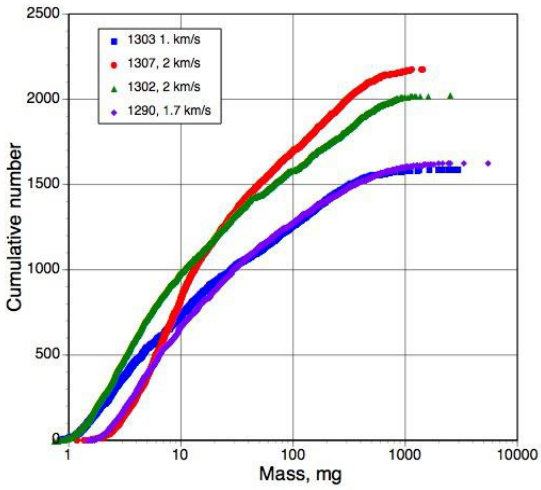

Figure 6. Number distribution of fragment mass.

In [3] it is assumed that the number of fragments varies as residual velocity squared. In these experiments, which were all well above the ballistic limit, this ratio will be very close to the impact velocity squared, or 1.38. The actual ratio is 1.31, which is rather close to the model.

The assumption that distributions for particle mass, direction, and shape are uncorrelated can also be evaluated from the data. Figure 7A is a scatter plot of particle mass vs. departure angle for a 2.0 km/s shot. For particles less than 10 mg, there is a clustering for cone angles less than ten degrees. These particles, however, have very little ability to penetrate components behind the armor. Larger particles do indeed appear uncorrelated with angle, as assumed by [2]. Similar results are obtained for mass and direction of steel fragments.

In the model of [2, 3] velocity is assumed to vary as the cosine of departure angle. That assumption is not validated by these data, except for the highest velocity particles. Below about 600 m/s, there is no correlation between velocity and departure angle.

The correlation between mass and shape for tungsten particles at 2.0 km/s is shown in Figure 7B. Here it appears that the smallest particles are a different population than the larger ones. For particles larger than about 50 mg, the shape is slightly elongated, which persists with a relatively large variance to particles in the gram size. Similar results are also obtained for steel particles; particles larger than about 12 mg are have aspect ratios of about two, but particles smaller than that have larger mean aspect ratios and a very large variance around the mean.

The velocity of particles may be assumed to be a monotonic function of p/d. It is linear for Poncelet penetration, and a square root dependence if the hole volume is proportional to kinetic energy. Therefore, in scatter plots vs. p/d, we can examine velocity correlations between parameters. Figure 8 is a plot of particle mass vs. p/d for tungsten particles from a 2 km/s shot. Most particles are relatively slow. The fastest particles are small. Thus, independent distribution for mass and velocity, as assumed in [2] and [3], is not supported by these data.

A more quantitative representation of particle velocity can be obtained by operating on the data with equation (1). Damage potential of particles is probably a function of their kinetic energy. Figure 9 shows the distribution of energy of tungsten particles for shots a 1.7 and a 2 km/s. These were obtained from equation (1), but particles that were estimated to have higher velocity than the initial velocity (about 20%) were omitted. Plots such as these may provide direct measurements of damage potential. The range of particle energies is considerably larger for the higher velocity impact.

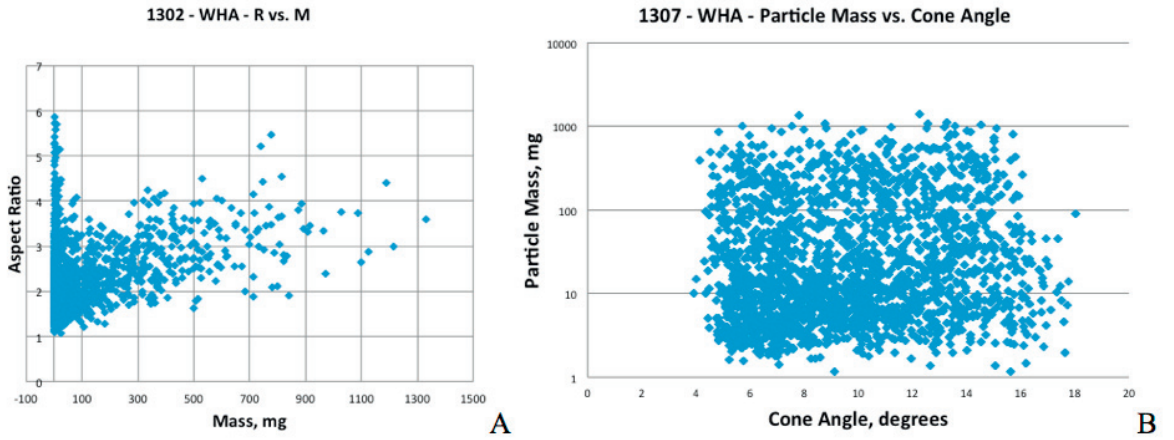

Figure 7. Correlation between mass and direction (A) and shape (B) for tungsten particles.

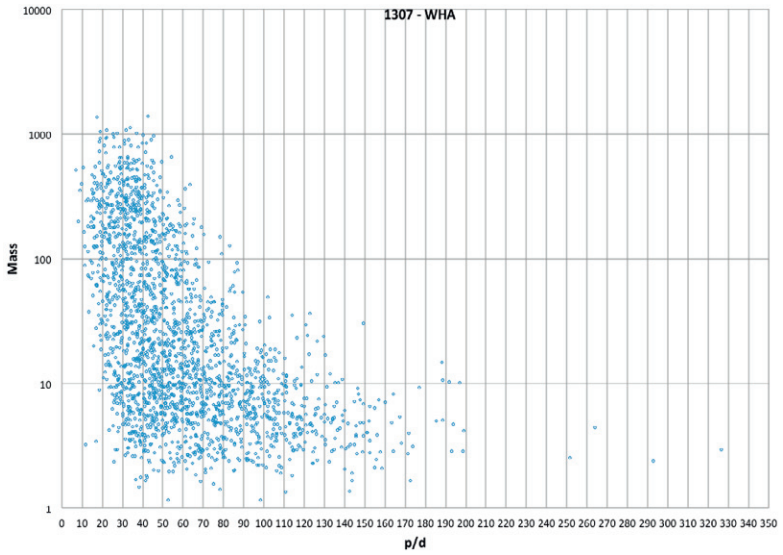

Figure 8. Mass vs. scaled depth for tungsten particles at 2 km/s.

Using the common assumption that a spherical projectile makes a hemispherical crater, and the volume of the crater is

$$P = (3E / 2R)^{1/3}$$

the projectile kinetic energy divided by R, where R is the spherical cavity expansion pressure (in Pa = J/m^3), then

If we make the reasonable assumption that particles that damage equipment must at least be able to penetrate 3 mm of aluminum, for which typically R = 2 GPa, then the required energy of a damaging particle is 36 J. As a filter, this requirement screens out most particles. Application of this filter applied to the data in Figure 9 finds that the number of particles with this critical energy is about equal for 1.7 and 2.0 km/s impacts. For any energy higher than this, there are

more particles from the lower velocity shot. Thus, as regards lethality as a function of velocity for CKE rods, it appears that for damage to relatively vulnerable components, higher velocity provides enhanced lethality, but the opposite is true for relatively hard components.

4. Modeling

The EPIC mesh-to-particle algorithm as described by Johnson et al. [7] was used to simulate these experiments. In this algorithm highly distorted elements are converted into particle nodes at a critical value of plastic strain. The dynamics of each particle node is determined by the interaction forces with a set of neighboring particles. Fragmentation occurs through separation of neighboring particle nodes. If a material failure model is employed it will effect the fragmentation process through the force calculation (the interaction force can only be repulsive between two failed particles).

Initial calculations were performed using the Johnson-Cook strength and failure models. Parameters in the EPIC library for armor steel and tungsten alloy were used. Subsequent calculations investigated a different failure model based on a maximum value for tensile stress as opposed to plastic strain. Comparisons with data were focused on fragments larger than 10 mg, since fragments with mass below this value are believed to have very little damage potential. The best agreement with experimental results for the fragment sizes was obtained when the code was run with no failure model at all. This result would tend to indicate that, within the context of the mesh-to-particle algorithm, fragmentation is better described by a competition between attractive potential energy and relative kinetic energy of adjacent material points rather than by excessive plastic strain or tensile stress. It is unclear whether this observation is simply a numerical artifact or whether it has a physical basis as well.

Figure 10 illustrates the agreement that was obtained with failure suppressed. The graph shows the fraction of particles with mass larger than a given value—both for experiment and in the code. For the larger particles that are responsible for damage, the agreement is quite satisfactory. The values of parameters used in this simulation were:

1. Mass of typical element of tungsten alloy ≈ 1–2 g.
2. Critical value of plastic strain = 0.4.
3. Dimensionless smoothing distance = 1.0.

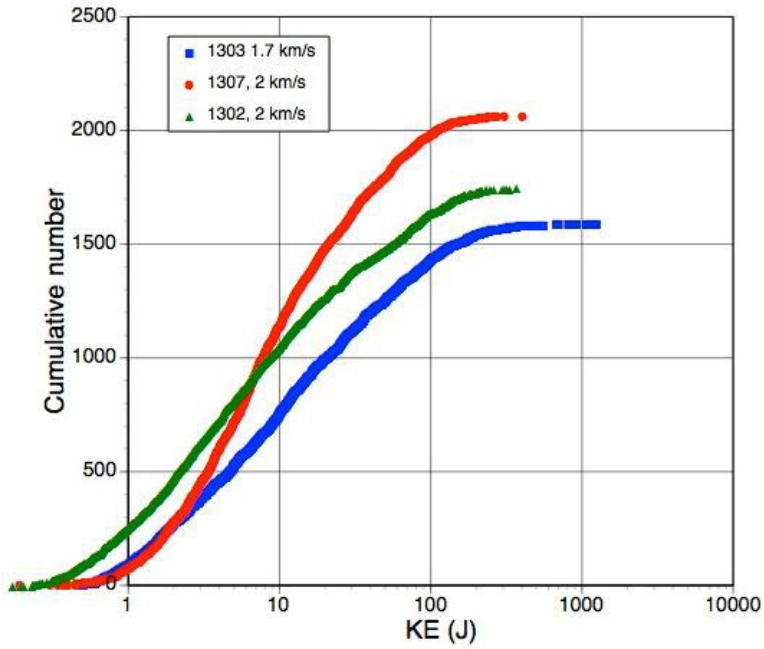

Figure 9. Approximate energy distribution of tungsten fragments

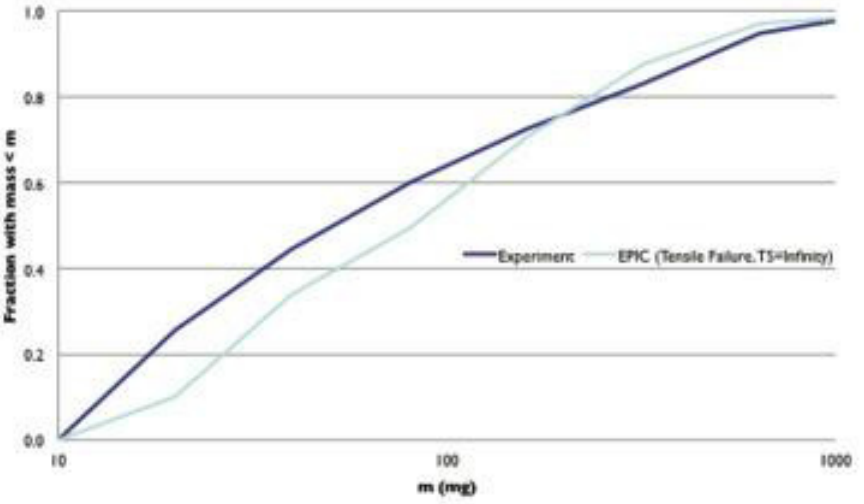

Figure 10. WHA fragment mass distribution (mass > 10 mg only). The calculation was run using no failure criteria for the tungsten alloy.

5. Conclusion

Particle capture combined with x-ray tomography provides a powerful tool to generate statistical data for BAD fragments. It is found that many key assumptions in standard modeling of debris are borne out by the data: most distributions can be approximated as Gaussian, and most parameters describing the distributions are not cross correlated. Increasing velocity from 1.7 to 2.0 km/s produces a greater number of faster fragments, but fewer fragments with higher energy. Observed fragment distributions could be simulated with EPIC using the mesh-to-particle routine with alternative failure criteria disabled.

Acknowledgment

The research reported in this document was performed in connection with Contract number W911QX-07-D-0002 with the U.S. Army Research Laboratory. The views and conclusions contained in this document are those of the authors and should not be interpreted as presenting the official policies or position, either expressed or implied, of the U.S. Army Research Laboratory or the U.S. Government unless so designated by other authorized documents. Citation of manufacturers or trade names does not constitute an official endorsement or approval of the use thereof. The U.S. Government is authorized to reproduce and distribute reprints for government purposes notwithstanding any copyright notation hereon.

References

[1] M. Mayseless, N. Sela, A. J. Stilp, V. Hohler, “Behind the Armor Debris Distribution Function,” Proc. 13the Int’l Symp. Ballistics Vol. 2, 77-85, Stockholm, Sweden, June 1992.
[2] R. Saucier, R. Shnidman, and J. Collins III, “A Stochastic Behind-Armor Debris Model,” 15th Int’l Symp. Ballistics, Jerusalem, Israel, 21–24 May 1995.
[3] R. Saucier, Behind Armor Debris Model, private communication, 11 December 2001.
[4] K. Weber, V. Hohler, K. Skeinschnitger, E. Schmolinske, and E. Schneider, “Debris Cloud Expansion Behind Oblique Single Plate Targets Perforated by Rod Projectiles,” 17th Int’l Symp Ballistics, Midrand, S.A., 23–27 March 1998.
[5] G. Yossifon and A. L. Yarin, “Behind-the-Armor Debris Analysis,” Int’l J. Impact Engng 27:807–836, 2002.
[6] D. Grady, “Local Inertial Effects in Dynamic Fragmentation,” J. Appl. Phys., 53:322–325, 1982.
[7] G. Johnson, R. Stryk, C. Gerlach, T. Holmquist, and N. Rowe, “A Quantitative Assessment of Computational Results for Behind Armor Debris,” 23rd Int’l Symp. Ballistics, Tarragona, Spain, April 2007.